

**On the graphical display of  
Powell-Sabin splines: a comparison of  
three piecewise linear approximations**

*Hendrik Speleers*

*Paul Dierckx*

*Stefan Vandewalle*

*Report TW 515, January 2008*



**Katholieke Universiteit Leuven**  
Department of Computer Science

Celestijnenlaan 200A – B-3001 Heverlee (Belgium)

# On the graphical display of Powell-Sabin splines: a comparison of three piecewise linear approximations

*Hendrik Speleers*

*Paul Dierckx*

*Stefan Vandewalle*

*Report TW 515, January 2008*

Department of Computer Science, K.U.Leuven

## **Abstract**

Powell-Sabin splines are  $C^1$ -continuous piecewise quadratic polynomials defined on arbitrary triangulations. They admit a compact representation in a normalized B-spline basis with a geometric interpretation involving control triangles. This paper discusses several piecewise linear approximations for the graphical display of Powell-Sabin splines. We analyse their approximation error to the spline surface, measured in the max-norm.

**Keywords :** Powell-Sabin splines, graphical display, wireframes

**MSC :** Primary : 65D07, Secondary : 65D17

# On the graphical display of Powell-Sabin splines: a comparison of three piecewise linear approximations

Hendrik Speleers\*, Paul Dierckx and Stefan Vandewalle

*Department of Computer Science, Katholieke Universiteit Leuven  
Celestijnenlaan 200A, B-3001 Leuven, Belgium*

## Abstract

Powell-Sabin splines are  $C^1$ -continuous piecewise quadratic polynomials defined on arbitrary triangulations. They admit a compact representation in a normalized B-spline basis with a geometric interpretation involving control triangles. This paper discusses several piecewise linear approximations for the graphical display of Powell-Sabin splines. We analyse their approximation error to the spline surface, measured in the max-norm.

*Keywords:* Powell-Sabin splines, graphical display, wireframes

*AMS classification:* 65D07, 65D17

## 1 Introduction

In computer aided geometric design it is often required or useful to construct a piecewise linear approximation of a given curve or surface, e.g., for efficient visualization, intersection testing, and geometric modelling. Such linear approximations are often realized through the use of refined control polygons [4]. Piecewise linear approximations have been extensively analysed for Bézier curves [11, 22, 10] and B-splines [9, 13].

In this paper we discuss and analyse several linear approximations of Powell-Sabin splines [14]. These  $C^1$ -continuous quadratic macro elements can be represented in a stable normalized B-spline basis. They have an intuitive geometric interpretation based on tangent control triangles. Vanraes *et al.* [19] considered a global subdivision scheme, which was extended to a local subdivision scheme in [15]. These properties are useful in a wide range of applications: Powell-Sabin splines are suited for geometric design [7, 18, 16] and data fitting [2].

In the literature of Powell-Sabin splines, several piecewise linear approximations are proposed for the graphical display of such splines. In this paper, we give an overview of these approximations, and we will analyse their convergence properties. In Section 2 we recall the definition of the Powell-Sabin spline space, and the construction of a normalized basis. Section 3 discusses three types of piecewise linear approximations. Finally, in Section 4 we end with some conclusions.

---

\*Research Assistant of the Fund for Scientific Research Flanders (Belgium)

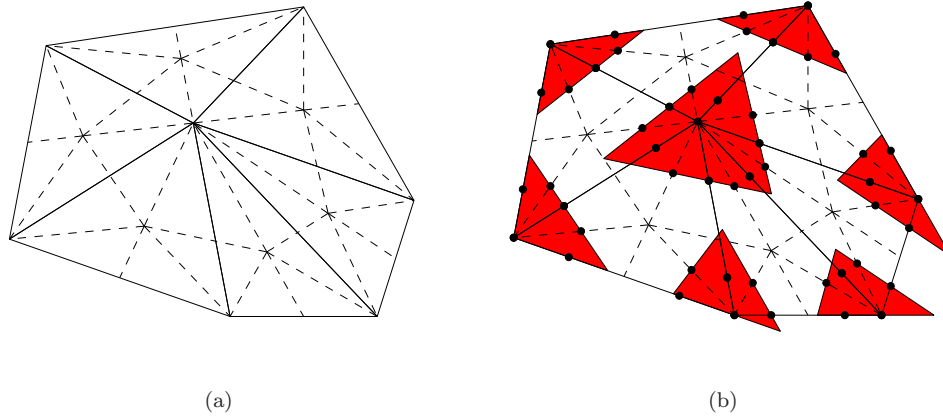


Figure 1: (a) A PS refinement  $\Delta^*$  (dashed lines) of a given triangulation  $\Delta$  (solid lines); (b) the PS points (bullets) and a set of suitable PS triangles (shaded).

## 2 Powell-Sabin splines

### 2.1 The Powell-Sabin spline space

Consider a simply connected subset  $\Omega \subset \mathbb{R}^2$  with polygonal boundary  $\partial\Omega$ . Assume a conforming triangulation  $\Delta$  of  $\Omega$  is given. A triangulation is conforming if no triangle contains a vertex different from its own three vertices. Let  $n$ ,  $t$  and  $e$  be the number of vertices, triangles and edges in the triangulation  $\Delta$ . Denote  $|\Delta|$  as the mesh size of  $\Delta$ , i.e., the length of the largest edge in  $\Delta$ .

The Powell-Sabin (PS) refinement  $\Delta^*$  partitions each triangle  $\rho_j \in \Delta$  into six subtriangles with a common vertex  $Z_j$ . This partition is defined algorithmically as follows:

1. Choose an interior point  $Z_j$  in each triangle  $\rho_j$ , so that if two different triangles  $\rho_i$  and  $\rho_j$  have a common edge, then the line joining  $Z_i$  and  $Z_j$  intersects the common edge at a point  $R_{ij}$  between its vertices.
2. Join each point  $Z_j$  to the vertices of  $\rho_j$ .
3. For each edge of the triangle  $\rho_j$ 
  - (a) which belongs to the boundary  $\partial\Omega$ : join  $Z_j$  to an arbitrary point in the interior of that edge;
  - (b) which is common to a triangle  $\rho_i$ : join  $Z_j$  to  $R_{ij}$ .

Figure 1(a) displays a triangulation with 6 triangles, and a corresponding PS refinement containing 36 subtriangles. Let  $\Pi_d$  be the space of bivariate polynomials of degree  $d$ . The space of piecewise quadratic polynomials on  $\Delta^*$  with global  $C^1$ -continuity is called the Powell-Sabin spline space:

$$S_2^1(\Delta^*) := \left\{ s \in C^1(\Omega) : s|_{\rho_j^*} \in \Pi_2, \rho_j^* \in \Delta^* \right\}. \quad (2.1)$$

Each of the  $6t$  triangles resulting from the PS refinement is the domain triangle of a quadratic bivariate polynomial. Powell and Sabin [14] proved that the following interpolation problem at each vertex  $V_k$

$$s(V_k) = f_k, \quad D_x s(V_k) = f_{x,k}, \quad D_y s(V_k) = f_{y,k}, \quad (2.2)$$

has a unique solution  $s(x, y) \in S_2^1(\Delta^*)$  for any given set of  $n$   $(f_k, f_{x,k}, f_{y,k})$ -values. It follows that the dimension of the Powell-Sabin spline space  $S_2^1(\Delta^*)$  is equal to  $3n$ .

## 2.2 A normalized B-spline representation

Dierckx [1] showed that each piecewise polynomial  $s(x, y) \in S_2^1(\Delta^*)$  has a unique representation

$$s(x, y) = \sum_{i=1}^n \sum_{j=1}^3 c_{i,j} B_i^j(x, y). \quad (2.3)$$

The basis functions  $B_i^j(x, y)$  have a local support, and they form a convex partition of unity, i.e.,

$$B_i^j(x, y) \geq 0, \quad \text{and} \quad \sum_{i=1}^n \sum_{j=1}^3 B_i^j(x, y) = 1. \quad (2.4)$$

Such a normalized basis can be constructed in a geometric way. We associate with each vertex  $V_i$  in the triangulation three linearly independent triplets  $(\alpha_{i,j}, \beta_{i,j}, \gamma_{i,j})$ ,  $j = 1, 2, 3$ . These triplets are determined as follows:

1. For each vertex  $V_i$ , identify the corresponding PS points. The PS points of  $V_i$  are defined as the midpoints of all edges in the PS refinement  $\Delta^*$  ending in  $V_i$ . The vertex  $V_i$  itself is also a PS point. In Figure 1(b) the PS points are indicated as bullets.
2. For each vertex  $V_i$ , find a triangle  $t_i(Q_{i,1}, Q_{i,2}, Q_{i,3})$  containing all the PS points of  $V_i$ . The triangles  $t_i$ ,  $i = 1, \dots, n$ , are called PS triangles. Note that these triangles are not uniquely defined. Figure 1(b) shows a possible set of PS triangles.
3. The three linearly independent triplets  $(\alpha_{i,j}, \beta_{i,j}, \gamma_{i,j})$ ,  $j = 1, 2, 3$ , are derived from the PS triangle  $t_i$  of a vertex  $V_i$  as follows:
  - $\alpha_i = (\alpha_{i,1}, \alpha_{i,2}, \alpha_{i,3})$  are the barycentric coordinates of  $V_i$  with respect to  $t_i$ ,
  - $\beta_i = (\beta_{i,1}, \beta_{i,2}, \beta_{i,3})$  and  $\gamma_i = (\gamma_{i,1}, \gamma_{i,2}, \gamma_{i,3})$  are the coordinates of the unit barycentric directions, in  $x$ - and  $y$ -direction respectively, with respect to  $t_i$ .

The Powell-Sabin B-spline  $B_i^j(x, y)$  is defined as the unique solution of interpolation problem (2.2) with all  $(f_k, f_{x,k}, f_{y,k}) = (0, 0, 0)$  except for  $k = i$ , where  $(f_i, f_{x,i}, f_{y,i}) = (\alpha_{i,j}, \beta_{i,j}, \gamma_{i,j}) \neq (0, 0, 0)$ . The condition of the B-spline basis is directly related to the size of the PS triangles. Typically, smaller PS triangles lead to a better conditioned basis.

The PS control points are defined as

$$\mathbf{c}_{i,j} = (Q_{i,j}, c_{i,j}), \quad (2.5)$$

and the PS control triangles as  $T_i(\mathbf{c}_{i,1}, \mathbf{c}_{i,2}, \mathbf{c}_{i,3})$ , which are tangent to the surface  $z = s(x, y)$  at the corresponding vertices  $V_i$ .

Vanraes *et al.* [19] developed a global subdivision scheme for Powell-Sabin splines. Subdivision is a procedure to represent a surface on a finer mesh than the mesh on which it is originally defined. The subdivision strategy for Powell-Sabin splines is based on the  $\sqrt{3}$ -refinement scheme of Kobbelt [8]. Applying this scheme twice, we obtain a triadic refinement. Every original edge is then trisected, and each original triangle is split into nine subtriangles. In Figure 2 the triadic subdivision scheme is illustrated for a given Powell-Sabin spline. This subdivision scheme is numerically stable, since only convex combinations are needed to compute the PS control points of the refined spline. The scheme was extended to a local subdivision scheme in [15].

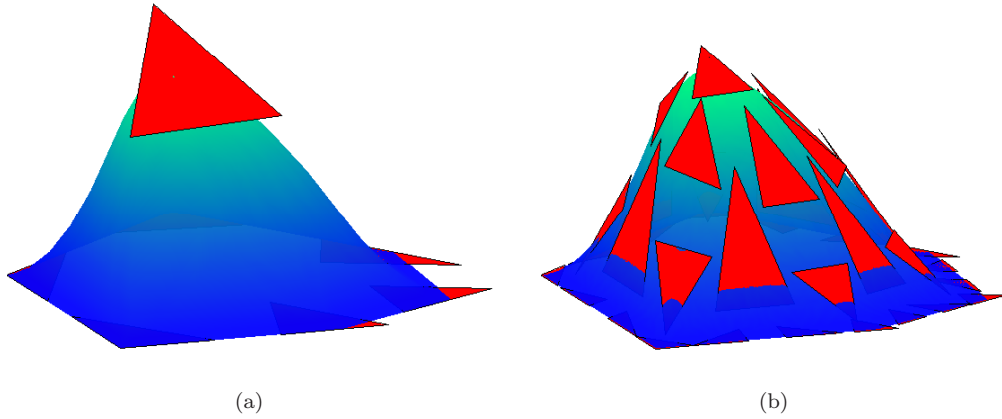


Figure 2: (a) A Powell-Sabin spline constructed by 7 PS control triangles on the triangulation in Figure 1; (b) the equivalent triadically subdivided spline with 37 PS control triangles.

### 3 Piecewise linear approximations

Subdivision is a common tool for the graphical display of splines. After a few subdivision steps, the PS control triangles approximate the shape of the Powell-Sabin spline quite well (see Figure 2). These control triangles can be used to construct a wireframe that mimics the spline surface. The question is how to connect the PS control triangles efficiently into a single wireframe. We consider three approaches of piecewise linear approximations. Figure 3 depicts the different wireframes for the Powell-Sabin spline in Figure 2. To analyse their convergence rates to the spline surface, we will derive an upper bound for the approximation errors, measured in the max-norm. For continuous piecewise polynomials, this norm is defined as

$$\|s\|_{\infty, \Omega} = \max_{(x,y) \in \Omega} |s(x,y)|. \quad (3.1)$$

We also need the following notation,

$$\|\nabla^2 s\|_{\infty, \Omega} = \max_{\rho^* \in \Delta^*} \left\| \max_{\|u\|=1, \|v\|=1} |D_u D_v(s)| \right\|_{\infty, \rho^*}, \quad (3.2)$$

where  $D_u$  and  $D_v$  are directional derivatives. For simplicity of the notation, we shall omit the subscript  $\Omega$  if the domain is obvious.

#### 3.1 A wireframe based on vertex interpolation

A first type of wireframe can be constructed by connecting the spline interpolation points  $s(V_i)$ , in the same way as the vertices  $V_i$  are connected in the domain triangulation  $\Delta$ . Note that the PS control triangles are tangent to the Powell-Sabin spline at these points. The value of such a point can be written as a convex combination of the control points, i.e.,

$$s(V_i) = \alpha_{i,1} c_{i,1} + \alpha_{i,2} c_{i,2} + \alpha_{i,3} c_{i,3}. \quad (3.3)$$

Here,  $(\alpha_{i,1}, \alpha_{i,2}, \alpha_{i,3})$  are the barycentric coordinates of vertex  $V_i$  with respect to the PS triangle  $t_i$ . The use of this wireframe for the graphical display of a Powell-Sabin spline was suggested in [21].

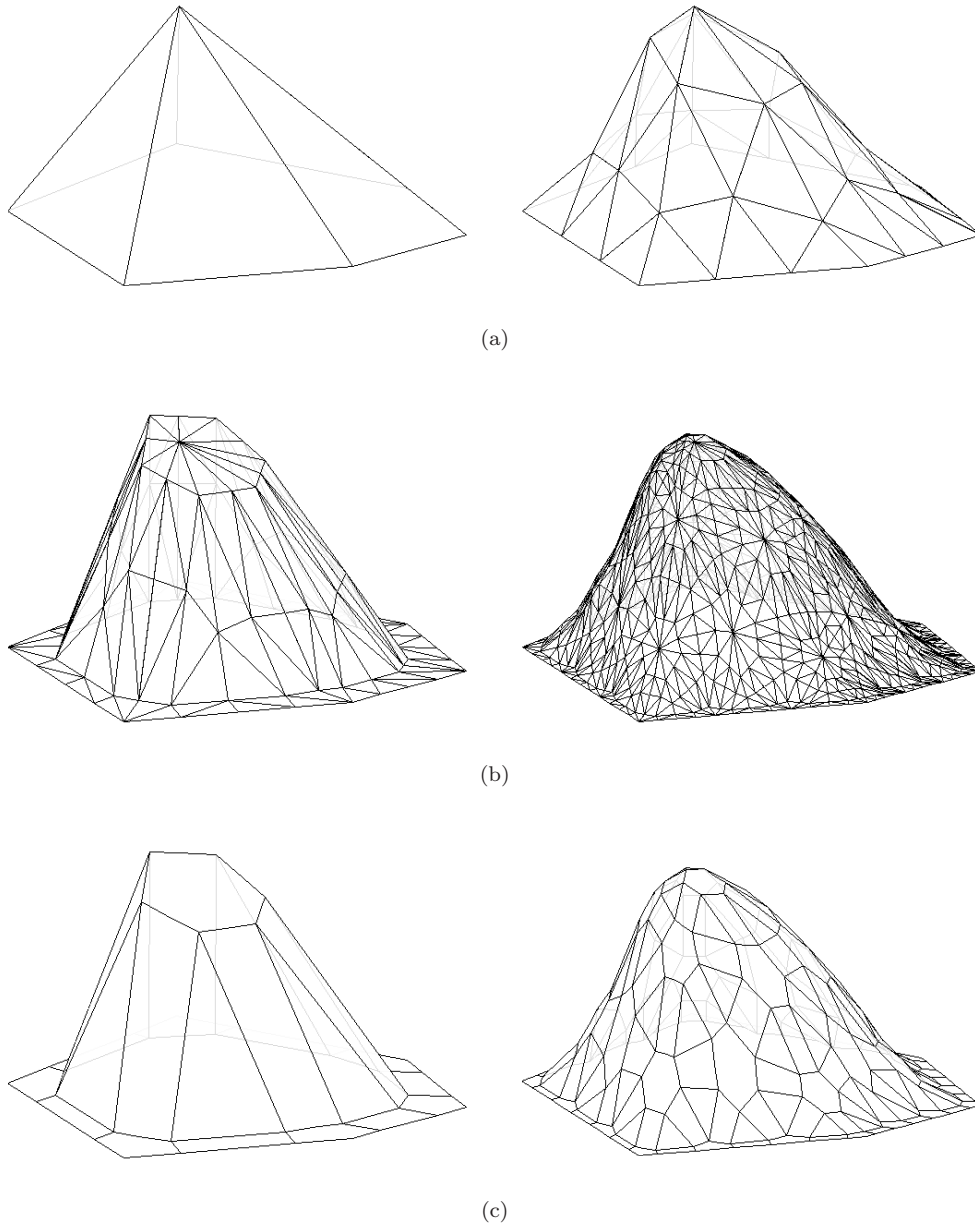


Figure 3: Different wireframes for the graphical display of the Powell-Sabin spline in Figure 2. They are obtained (a) by connecting the spline interpolation points  $s(V_i)$ , (b) by using the Bézier net, (c) by connecting the projections of certain PS points into the corresponding PS control triangles, as explained in Section 3.3.

It is illustrated in Figure 3(a) for the spline in Figure 2. For future reference, we shall denote this linear interpolant as  $\Gamma_1(s)$ .

The following theorem treats the convergence of  $\Gamma_1(s)$  to the Powell-Sabin spline  $s(x, y)$ . Stämpfle [17] proved that the error of linear interpolation at the vertices for a  $C^1$ -continuous function on a triangle  $\rho$  behaves, in general, as  $\mathcal{O}(|\rho|)$ . Although the Powell-Sabin spline is  $C^1$ -continuous on each triangle in the triangulation  $\Delta$ , we can show that the error converges quadratically in the mesh size. Recall that the mesh size is the length of the largest edge in the triangulation.

**Theorem 1.** *The linear interpolant  $\Gamma_1(s)$  converges to the Powell-Sabin spline  $s(x, y)$  as*

$$\|\Gamma_1(s) - s\|_\infty \leq \frac{2}{3} |\Delta^*|^2 \|\nabla^2 s\|_\infty, \quad (3.4)$$

with  $|\Delta^*|$  the mesh size of the PS refinement  $\Delta^*$ .

*Proof.* Consider a triangle  $\rho \in \Delta$  with given subtriangles  $\rho^* \in \Delta^*$ , see Figure 4(a) for a graphical illustration. We first show that the error of the linear interpolant and the Powell-Sabin spline at each vertex  $W$  in the PS refinement can be bounded by

$$|(\Gamma_1(s) - s)(W)| \leq \frac{|\Delta^*|^2}{2} \|\nabla^2 s\|_{\infty, \rho}. \quad (3.5)$$

Because of the interpolation, the error is zero at the three vertices  $V_i, V_j$  and  $V_k$  of triangle  $\rho$ . We will prove inequality (3.5) for the point  $R_{ij} = \lambda_{ij} V_i + \lambda_{ji} V_j$ . The proof is similar for the other points in the the PS refinement (i.e.,  $R_{jk}, R_{ki}$  and  $Z_{ijk}$ ). Let  $\tilde{S}(u)$  be the univariate (piecewise) quadratic spline corresponding to  $s(x, y)$  along the edge  $V_j - V_i$ , with  $u$  the accumulated  $l_2$ -length parameter along this edge from  $V_i$  towards  $V_j$ . Let  $u_i, u_{ij}$  and  $u_j$  be the values corresponding to  $V_i, R_{ij}$  and  $V_j$ , respectively. From the Taylor expansions at  $u_i$  and  $u_j$  we know that

$$\tilde{S}(u_{ij}) = \tilde{S}(u_i) + (u_{ij} - u_i) D(\tilde{S})(u_i) + \frac{(u_{ij} - u_i)^2}{2} D^2(\tilde{S})(u_i), \quad (3.6)$$

$$\tilde{S}(u_{ij}) = \tilde{S}(u_j) + (u_{ij} - u_j) D(\tilde{S})(u_j) + \frac{(u_{ij} - u_j)^2}{2} D^2(\tilde{S})(u_j). \quad (3.7)$$

Since the spline  $\tilde{S}(u)$  is a quadratic polynomial on  $u_{ij} - u_i$ , we can write that

$$D(\tilde{S})(u_{ij}) = \frac{2}{(u_{ij} - u_i)} (\tilde{S}(u_{ij}) - \tilde{S}(u_i)) - D(\tilde{S})(u_i), \quad (3.8)$$

and, analogously, on  $u_j - u_{ij}$  we have

$$D(\tilde{S})(u_{ij}) = \frac{2}{(u_{ij} - u_j)} (\tilde{S}(u_{ij}) - \tilde{S}(u_j)) - D(\tilde{S})(u_j). \quad (3.9)$$

By the  $C^1$ -continuity of the spline at  $u_{ij}$ , the right hand sides of (3.8) and (3.9) are equal to each other. In combination with the equality  $\lambda_{ij}(u_{ij} - u_i) + \lambda_{ji}(u_{ij} - u_j) = 0$ , we obtain that

$$\lambda_{ij} \left( \tilde{S}(u_{ij}) - \tilde{S}(u_i) - \frac{(u_{ij} - u_i)}{2} D(\tilde{S})(u_i) \right) = -\lambda_{ji} \left( \tilde{S}(u_{ij}) - \tilde{S}(u_j) - \frac{(u_{ij} - u_j)}{2} D(\tilde{S})(u_j) \right),$$

and, using  $\lambda_{ij} + \lambda_{ji} = 1$ , it follows

$$\tilde{S}(u_{ij}) = \lambda_{ij} \left( \tilde{S}(u_i) + \frac{(u_{ij} - u_i)}{2} D(\tilde{S})(u_i) \right) + \lambda_{ji} \left( \tilde{S}(u_j) + \frac{(u_{ij} - u_j)}{2} D(\tilde{S})(u_j) \right). \quad (3.10)$$

Taking a linear combination of the previous equations (3.6), (3.7) and (3.10) we have

$$\begin{aligned}\tilde{S}(u_{ij}) &= 2\tilde{S}(u_{ij}) - \lambda_{ij}\tilde{S}(u_{ij}) - \lambda_{ji}\tilde{S}(u_{ij}) \\ &= \lambda_{ij}\left(\tilde{S}(u_i) - \frac{(u_{ij} - u_i)^2}{2}D^2(\tilde{S})(u_i)\right) + \lambda_{ji}\left(\tilde{S}(u_j) - \frac{(u_{ij} - u_j)^2}{2}D^2(\tilde{S})(u_j)\right).\end{aligned}$$

Because  $\Gamma_1(\tilde{S}(u_{ij})) = \lambda_{ij}\tilde{S}(u_i) + \lambda_{ji}\tilde{S}(u_j)$ , we find the relation

$$\Gamma_1(\tilde{S}(u_{ij})) - \tilde{S}(u_{ij}) = \lambda_{ij}\frac{(u_{ij} - u_i)^2}{2}D^2(\tilde{S})(u_i) + \lambda_{ji}\frac{(u_{ij} - u_j)^2}{2}D^2(\tilde{S})(u_j). \quad (3.11)$$

Since  $\lambda_{ij} + \lambda_{ji} = 1$ , we get inequality (3.5). Note that the proof of (3.5) for the interior point  $Z_{ijk} = z_iV_i + z_jV_j + z_kV_k$  is similar. In this case, the right hand side of equality (3.11) will be a linear combination of  $z_i$ ,  $z_j$  and  $z_k$ , instead of  $\lambda_{ij}$  and  $\lambda_{ji}$ .

We now prove error bound (3.4) on each of the six subtriangles  $\rho^*(W_1, W_2, W_3)$  of  $\rho$  in  $\Delta^*$ . We start by stating the following triangle inequality

$$|\Gamma_1(s) - s| \leq |\Gamma_1(s) - F| + |F - s|, \quad (3.12)$$

with function  $F$  defined as the linear interpolant over  $\rho^*$  through the points  $s(W_1)$ ,  $s(W_2)$  and  $s(W_3)$  of the spline surface, i.e.,

$$F(x, y) = \tau_1 s(W_1) + \tau_2 s(W_2) + \tau_3 s(W_3).$$

The triplet  $(\tau_1, \tau_2, \tau_3)$  are the barycentric coordinates of the point  $(x, y)$  with respect to triangle  $\rho^*$ . Both terms in the right hand side of (3.12) will be bounded independently. Because  $\Gamma_1(s)$  is linear on  $\rho^*$ , we have

$$\Gamma_1(s) - F = \tau_1(\Gamma_1(s) - s)(W_1) + \tau_2(\Gamma_1(s) - s)(W_2) + \tau_3(\Gamma_1(s) - s)(W_3).$$

Since the barycentric coordinates are positive and sum up to one, it follows that

$$|\Gamma_1(s) - F| \leq \max\{|\Gamma_1(s) - s)(W_1)|, |\Gamma_1(s) - s)(W_2)|, |\Gamma_1(s) - s)(W_3)|\}.$$

By (3.5) we get

$$|\Gamma_1(s) - F| \leq \frac{|\Delta^*|^2}{2} \|\nabla^2 s\|_\infty. \quad (3.13)$$

The second term in the right hand side of (3.12) is the error of a linear interpolant at the vertices of triangle  $\rho^*$ . We know from [20, 17] that such an interpolation error for  $C^2$ -continuous functions can be estimated as

$$|F - s| \leq \frac{|\rho^*|^2}{6} \|\nabla^2 s\|_\infty. \quad (3.14)$$

Filling the estimates (3.13)-(3.14) into (3.12) results in (3.4).  $\square$

**Remark 2.** *Figure 7(a) illustrates the convergence of the wireframe  $\Gamma_1(s)$  to the corresponding Powell-Sabin spline. We used the wireframes of the spline in Figure 2(a) and four subdivided equivalent splines. The maximum error, the mean error and upper bound (3.4) are plotted in the figure.*

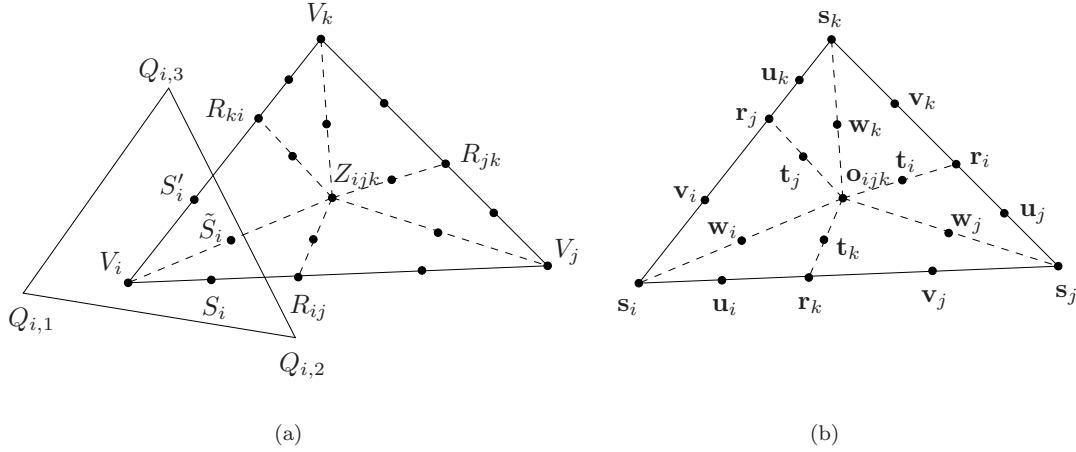


Figure 4: (a) PS refinement of triangle  $\rho(V_i, V_j, V_k)$  together with PS triangle  $t_i(Q_{i,1}, Q_{i,2}, Q_{i,3})$  of vertex  $V_i$ ; (b) position of the Bézier control points of a Powell-Sabin spline in its Bernstein-Bézier representation.

### 3.2 The Bézier net

A second type of wireframe can be obtained by using the Bézier net of the Powell-Sabin spline in its Bernstein-Bézier representation, as suggested in [1].

The Bézier net can be constructed as follows. We consider a triangle  $\rho(V_i, V_j, V_k)$  in the triangulation  $\Delta$  with its PS refinement in  $\Delta^*$ . The other triangles in  $\Delta$  are treated in the same way. We assume that the points shown in Figure 4(a) have the following barycentric coordinates:  $V_i(1, 0, 0)$ ,  $V_j(0, 1, 0)$ ,  $V_k(0, 0, 1)$ ,  $Z_{ijk}(z_i, z_j, z_k)$ ,  $R_{ij}(\lambda_{ij}, \lambda_{ji}, 0)$ ,  $R_{jk}(0, \lambda_{jk}, \lambda_{kj})$ , and  $R_{ki}(\lambda_{ik}, 0, \lambda_{ki})$ . On each of the six triangles in  $\Delta^*$  the Powell-Sabin spline (2.3) is a quadratic polynomial, that can be represented in its Bernstein-Bézier formulation by means of Bézier control points [3]. Their positions, the so-called domain points, are schematically illustrated in Figure 4(b). The  $z$ -coordinates of the Bézier control points are called Bézier ordinates. The Bézier control points are computed as

$$\mathbf{s}_i = \alpha_{i,1} \mathbf{c}_{i,1} + \alpha_{i,2} \mathbf{c}_{i,2} + \alpha_{i,3} \mathbf{c}_{i,3}, \quad (3.15a)$$

$$\mathbf{u}_i = L_{i,1} \mathbf{c}_{i,1} + L_{i,2} \mathbf{c}_{i,2} + L_{i,3} \mathbf{c}_{i,3}, \quad (3.15b)$$

$$\mathbf{v}_i = L'_{i,1} \mathbf{c}_{i,1} + L'_{i,2} \mathbf{c}_{i,2} + L'_{i,3} \mathbf{c}_{i,3}, \quad (3.15c)$$

$$\mathbf{w}_i = \tilde{L}_{i,1} \mathbf{c}_{i,1} + \tilde{L}_{i,2} \mathbf{c}_{i,2} + \tilde{L}_{i,3} \mathbf{c}_{i,3}. \quad (3.15d)$$

The values  $(\alpha_{i,1}, \alpha_{i,2}, \alpha_{i,3})$ ,  $(L_{i,1}, L_{i,2}, L_{i,3})$ ,  $(L'_{i,1}, L'_{i,2}, L'_{i,3})$  and  $(\tilde{L}_{i,1}, \tilde{L}_{i,2}, \tilde{L}_{i,3})$  are the barycentric coordinates of the PS points  $V_i$ ,  $S_i$ ,  $S'_i$ , and  $\tilde{S}_i$  with respect to the PS triangle  $t_i(Q_{i,1}, Q_{i,2}, Q_{i,3})$ . The other Bézier control points can be found from the continuity conditions of the Powell-Sabin spline, e.g.,

$$\mathbf{r}_k = \lambda_{ij} \mathbf{u}_i + \lambda_{ji} \mathbf{v}_j, \quad (3.15e)$$

$$\mathbf{t}_k = \lambda_{ij} \mathbf{w}_i + \lambda_{ji} \mathbf{w}_j, \quad (3.15f)$$

$$\mathbf{o}_{ijk} = z_i \mathbf{w}_i + z_j \mathbf{w}_j + z_k \mathbf{w}_k. \quad (3.15g)$$

The piecewise linear interpolant of the Bézier control points is called the Bézier control net. This control net is tangent to the spline surface at the vertices in the PS refinement, i.e., at the points  $V_i$ ,  $V_j$ ,  $V_k$ ,  $R_{ij}$ ,  $R_{jk}$ ,  $R_{ki}$  and  $Z_{ijk}$ . We denote the Bézier net of a Powell-Sabin spline  $s(x, y)$  as  $\Gamma_2(s)$ , and it is illustrated in Figure 3(b).

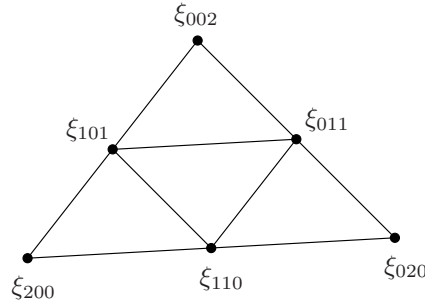


Figure 5: Position of the domain points  $\xi_{ijk}$  with  $i + j + k = 2$ .

The next theorem gives an upper bound for the error between the Bézier net and the underlying Powell-Sabin spline, measured in the max-norm.

**Theorem 3.** *The Bézier net  $\Gamma_2(s)$  converges to the Powell-Sabin spline  $s(x, y)$  as*

$$\|\Gamma_2(s) - s\|_\infty \leq \frac{|\Delta^*|^2}{6} \|\nabla^2 s\|_\infty, \quad (3.16)$$

with  $|\Delta^*|$  the mesh size of the PS refinement  $\Delta^*$ .

*Proof.* Consider a triangle  $\rho^* \in \Delta^*$  and the quadratic Bernstein-Bézier polynomial representation  $B(x, y)$  of the given Powell-Sabin spline  $s(x, y)$  on  $\rho^*$ . Denote its Bézier ordinates as  $b_{ijk}$  and its domain points as  $\xi_{ijk}$ , with  $i + j + k = 2$ . We use the notation from Farin [3] for the indices, and it is illustrated in Figure 5.

We first prove that the difference between the Bézier ordinates and the value of the polynomial at the corresponding domain points can be bounded as

$$|b_{ijk} - B(\xi_{ijk})| \leq \frac{|\rho^*|^2}{8} \|\nabla^2 B\|_{\infty, \rho^*}. \quad (3.17)$$

The difference is zero at the three corners of the triangle  $\rho^*$ , i.e.,  $b_{200} = B(\xi_{200})$ ,  $b_{020} = B(\xi_{020})$  and  $b_{002} = B(\xi_{002})$ . We now consider the domain point  $\xi_{110}$ . The reasoning is similar for the points  $\xi_{011}$  and  $\xi_{101}$ . Denote  $u$  as the accumulated  $l_2$ -length parameter along the edge of the triangle on which  $\xi_{110}$  is situated. Let  $\tilde{B}(u)$  be the trace of  $B(x, y)$  on this edge, and let  $u_{200}$ ,  $u_{110}$  and  $u_{020}$  be the points corresponding to  $\xi_{200}$ ,  $\xi_{110}$  and  $\xi_{020}$ . Considering the quadratic nature of  $\tilde{B}(u)$ , it is easy to check that

$$\begin{aligned} \tilde{B}(u_{110}) &= \frac{1}{4}(b_{200} + 2b_{110} + b_{020}), \\ D^2(\tilde{B})(u_{110}) &= \frac{2}{(u_{200} - u_{020})^2}(b_{200} - 2b_{110} + b_{020}). \end{aligned}$$

Hence,

$$\tilde{B}(u_{110}) - b_{110} = \frac{(u_{200} - u_{020})^2}{8} D^2(\tilde{B})(u_{110}),$$

from which we obtain the inequality (3.17).

We now prove inequality (3.16) by showing that it holds on the four subtriangles of triangle  $\rho^*$ :  $\rho(\xi_{200}, \xi_{110}, \xi_{101})$ ,  $\rho(\xi_{020}, \xi_{011}, \xi_{110})$ ,  $\rho(\xi_{002}, \xi_{101}, \xi_{011})$  and  $\rho(\xi_{110}, \xi_{011}, \xi_{101})$ . We only consider the

case on subtriangle  $\rho(\xi_{200}, \xi_{110}, \xi_{101})$ . The other cases are proven analogously. We start from the triangle inequality

$$|\Gamma_2(B) - B| \leq |\Gamma_2(B) - F| + |F - B|, \quad (3.18)$$

with function  $F$  defined as

$$F(x, y) = \tau_1 B(\xi_{200}) + \tau_2 B(\xi_{110}) + \tau_3 B(\xi_{101}).$$

The triplet  $(\tau_1, \tau_2, \tau_3)$  is the set of barycentric coordinates of the point  $(x, y)$  with respect to subtriangle  $\rho(\xi_{200}, \xi_{110}, \xi_{101})$ . By the definition of the Bézier net, we have

$$\Gamma_2(B) - F = \tau_1 (b_{200} - B(\xi_{200})) + \tau_2 (b_{110} - B(\xi_{110})) + \tau_3 (b_{101} - B(\xi_{101})).$$

By (3.17) it follows that

$$|\Gamma_2(B) - F| \leq \frac{|\rho^*|^2}{8} \|\nabla^2 B\|_{\infty, \rho^*}. \quad (3.19)$$

The second term in the right hand side of (3.18) can be bounded by (see [20, 17])

$$|F - B| \leq \frac{|\rho(\xi_{200}, \xi_{110}, \xi_{101})|^2}{6} \|\nabla^2 B\|_{\infty, \rho^*} = \frac{|\rho^*|^2}{24} \|\nabla^2 B\|_{\infty, \rho^*}. \quad (3.20)$$

Combining the estimates (3.19)-(3.20) with (3.18) results in (3.16).  $\square$

**Remark 4.** *The convergence of the wireframe  $\Gamma_2(s)$  is illustrated in Figure 7(b). We constructed the Bézier nets for the spline in Figure 2(a) and some subdivided equivalent splines. The graphs of the maximum error, the mean error and upper bound (3.16) are depicted in the figure.*

**Remark 5.** *Comparing the upper bounds (3.4) and (3.16), we note that the latter upper bound for the error of the Bézier net is four times smaller than the one for the vertex interpolation wireframe. This factor is also observed in the numerical experiments. For instance, the maximum error for the finest wireframe in Figure 7(b) is 3.29 times smaller than the corresponding one in Figure 7(a). The ratio of the mean error for the finest wireframes in both figures is 5.52.*

**Remark 6.** *The Bézier net provides a better linear approximation for the underlying spline than the vertex interpolation wireframe. A disadvantage, however, is that many triangular patches are needed in this representation. Since the Bézier net is constructed of four patches on each triangle in the PS refinement (see Figure 5), there are globally needed  $24t$  patches with  $t$  the number of triangles in the triangulation  $\Delta$ .*

**Remark 7.** *When a finer resolution for the Bézier net is required, one can apply the PS subdivision rules and calculate the Bernstein-Bézier representation of the refined Powell-Sabin spline. A more efficient approach for obtaining a finer wireframe is to keep the Bernstein-Bézier representation of the original spline and to use the Bézier subdivision rules for refining the Bézier net [6, 12, 5]. In this way, the refined Bézier control points are easy to compute.*

### 3.3 The reduced Bézier net

The third type of wireframe is a fair compromise between the two previous wireframes: it is based on the Bézier net, but it uses far less patches. The wireframe is constructed by connecting projections of some PS points into the PS control triangles in a way that will be explained below. Figure 3(c) shows such a wireframe for the Powell-Sabin spline in Figure 2.

To obtain this wireframe, we first build a certain mesh in the parameter domain. Subsequently, the points in the mesh are projected into the corresponding PS control triangles. The constructed mesh has three types of patches, as illustrated in Figure 6. The first type is associated with each

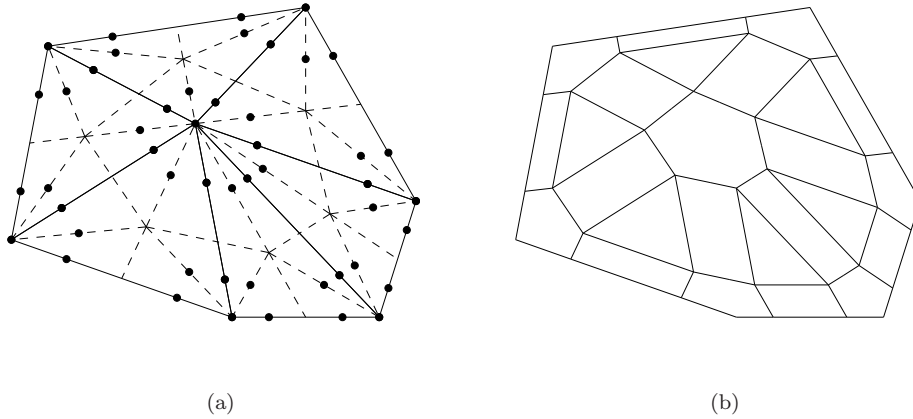


Figure 6: (a) A triangulation with PS refinement and PS points. (b) The mesh used for constructing the reduced Bézier net.

vertex  $V_i$ . It is obtained by constructing the smallest envelope polygon that contains all PS points associated with  $V_i$ . Obviously, the corners of such a polygon are PS points. Then, these corners are connected into triangular and quadrilateral patches in the following way. For each triangle in the domain triangulation  $\Delta$  we construct a triangular patch by connecting the three PS points in the interior of the considered triangle. We connect the adjacent PS points along each edge in  $\Delta$  to form a quadrilateral patch. The wireframe is then defined by the projections of the corners of these patches into the corresponding PS control triangles.

We shall call this wireframe the reduced Bézier net. Comparing the wireframes in Figures 3(b) and 3(c), one can see that the edges of the latter wireframe coincide with particular edges in the Bézier net. Many neighbouring patches in the Bézier net are coplanar. These patches are merged into a single patch in the reduced Bézier net. We denote the linear interpolant of this wireframe as  $\Gamma_3(s)$ . Obviously, we obtain the same convergence result as for the Bézier net.

**Theorem 8.** *The reduced Bézier net  $\Gamma_3(s)$  converges to the Powell-Sabin spline  $s(x, y)$  as*

$$\|\Gamma_3(s) - s\|_\infty \leq \frac{|\Delta^*|^2}{6} \|\nabla^2 s\|_\infty, \quad (3.21)$$

with  $|\Delta^*|$  the mesh size of the PS refinement  $\Delta^*$ .

**Remark 9.** *The convergence of the wireframe  $\Gamma_3(s)$  to the corresponding Powell-Sabin spline is analogous to the one of the Bézier net  $\Gamma_2(s)$ . The maximum error, the mean error and upper bound (3.21) are also illustrated in Figure 7(b).*

**Remark 10.** *The number of used patches is about 1/8 of the number needed for the Bézier net. More precisely, the wireframe consists of  $n + t + e$  patches, where  $n$ ,  $t$  and  $e$  are the number of vertices, triangles and edges, respectively, in the triangulation  $\Delta$ . Using Euler's formulas, the number of patches amounts to about  $3t$ . Because of the smaller number of patches, this wireframe is more visually pleasing than the Bézier net. Still it preserves the approximation properties of the Bézier net. A disadvantage is that the patches are constructed of polygons with a different number of edges.*

**Remark 11.** *All error estimates derived in this paper are given for arbitrary triangulations. Whereas the most approximation bounds in the finite element literature have a dependence on the*

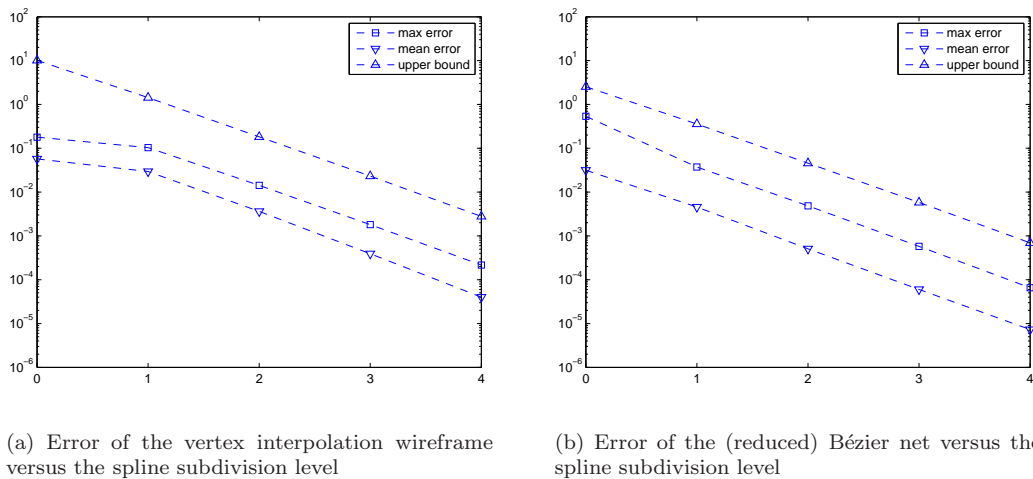


Figure 7: Convergence of the error of (a) the vertex interpolation wireframe and (b) the (reduced) Bézier net, computed for the spline in Figure 2(a) and several triadically subdivided versions. The graphs of the maximum error, the mean error and the estimated upper bound are shown.

wireframe	$c$	$p$
Vertex interpolation	$2/3$	$t$
Bézier net	$1/6$	$24t$
Reduced Bézier net	$1/6$	$n + t + e \sim 3t$

Table 1: Comparison of the three discussed wireframes for the graphical display of a Powell-Sabin spline  $s(x, y)$ . The second column gives the constant  $c$  in the upper bound  $c|\Delta^*|^2\|\nabla^2 s\|_\infty$  for the error measured in the max-norm. The third column denotes the number of patches  $p$  needed in the wireframe, assuming that the spline is defined on a triangulation  $\Delta$  with  $n$  vertices,  $t$  triangles and  $e$  edges.

*smallest angle in the triangulation, our estimates are all independent of the shape of the triangles in the given triangulation.*

## 4 Concluding remarks

We discussed three types of piecewise linear approximations for Powell-Sabin splines: the wireframe based on vertex interpolation, the Bézier net, and the reduced Bézier net. We derived an upper bound for the error of these wireframes measured in the max-norm, and we illustrated numerically their convergence rates to the spline surface. Table 1 summarizes the upper bounds, together with the number of patches needed in the wireframes.

Asymptotically, the wireframes converge to the spline surface as  $\mathcal{O}(|\Delta^*|^2)$ . The Bézier net and the reduced Bézier net are more accurate than the vertex interpolation wireframe. The latter, on the other hand, needs fewer triangular patches. The reduced Bézier net is visually the most attractive wireframe, since it approximates the shape of the Powell-Sabin spline quite well with a reasonable number of patches. A possible disadvantage is that this wireframe is composed of polygons with

a different number of edges. If the used graphical library cannot handle such polygons efficiently, then vertex interpolation may be recommended: it is fairly easy to construct with a small number of patches. The Bézier net is particularly interesting if the Bernstein-Bézier representation is already available or required for other purposes, e.g., for the evaluation or differentiation of the Powell-Sabin spline. A fine wireframe can then be obtained using the Bézier subdivision rules, but at the cost of a large set of patches.

## References

- [1] P. Dierckx. On calculating normalized Powell-Sabin B-splines. *Comput. Aided Geom. Design*, 15(1):61–78, 1997.
- [2] P. Dierckx, S. Van Leemput, and T. Vermeire. Algorithms for surface fitting using Powell-Sabin splines. *IMA J. Numer. Anal.*, 12:271–299, 1992.
- [3] G. Farin. Triangular Bernstein-Bézier patches. *Comput. Aided Geom. Design*, 3(2):83–127, 1986.
- [4] G. Farin. *Curves and Surfaces for CAGD: A Practical Guide*. Morgan Kaufmann Publishers, San Francisco, fifth edition, 2002.
- [5] J. Gallier. On the efficiency of strategies for subdividing polynomial triangular surface patches. Technical report, Dept. Computer and Information Science, University of Pennsylvania, 2006.
- [6] R. Goldman. Subdivision algorithms for Bézier triangles. *Comput. Aided Design*, 15:159–166, 1983.
- [7] Y. He, M. Jin, X. Gu, and H. Qin. A  $C^1$  globally interpolatory spline of arbitrary topology. In N. Paragios, O.D. Faugeras, T. Chan, and C. Schnörr, editors, *Proc. 3rd IEEE Workshop on Variational, Geometric and Level Set Methods in Computer Vision*, pages 295–306, Beijing, China, 2005.
- [8] L. Kobbelt.  $\sqrt{3}$ -Subdivision. In *Computer Graphics Proceedings*, Annual Conference Series, pages 103–112. ACM SIGGRAPH, 2000.
- [9] D. Lutterkort and J. Peters. Tight linear envelopes for splines. *Numer. Math.*, 89:735–748, 2001.
- [10] W. Ma and R. Zhang. Efficient piecewise linear approximation of Bézier curves with improved sharp error bound. In M.S. Kim and K. Shimada, editors, *Proc. Geometric Modeling and Processing, Pittsburgh 2006*, pages 157–174. Springer-Verlag, 2006.
- [11] D. Nairn, J. Peters, and D. Lutterkort. Sharp, quantitative bounds on the distance between a polynomial piece and its Bézier control polygon. *Comput. Aided Geom. Design*, 16(7):613–631, 1999.
- [12] J. Peters. Evaluation and approximate evaluation of the multivariate Bernstein-Bézier form on a regularly partitioned simplex. *ACM Trans. Math. Softw.*, 20:460–480, 1994.
- [13] J. Peters. Efficient one-sided linearization of spline geometry. In M.J. Wilson and R.R. Martin, editors, *Proc. 10th IMA Conf. on Mathematics of Surfaces*, pages 297–319. Springer-Verlag, 2003.
- [14] M.J.D. Powell and M.A. Sabin. Piecewise quadratic approximations on triangles. *ACM Trans. Math. Softw.*, 3:316–325, 1977.

- [15] H. Speleers, P. Dierckx, and S. Vandewalle. Local subdivision of Powell-Sabin splines. *Comput. Aided Geom. Design*, 23(5):446–462, 2006.
- [16] H. Speleers, P. Dierckx, and S. Vandewalle. Weight control for modelling with NURPS surfaces. *Comput. Aided Geom. Design*, 24(3):179–186, 2007.
- [17] M. Stämpfle. Optimal estimates for the linear interpolation error on simplices. *J. Approx. Theory*, 103:78–90, 2000.
- [18] E. Vanraes and A. Bultheel. Modelling sharp features with tangent subdivision. In M. Dæhlen, K. Mörken, and L.L. Schumaker, editors, *Proc. 6th Int. Conf. on Mathematical Methods for Curves and Surfaces*, pages 362–372. Nashboro Press, 2005.
- [19] E. Vanraes, J. Windmolders, A. Bultheel, and P. Dierckx. Automatic construction of control triangles for subdivided Powell-Sabin splines. *Comput. Aided Geom. Design*, 21(7):671–682, 2004.
- [20] S. Waldron. The error in linear interpolation at the vertices of a simplex. *SIAM J. Numer. Anal.*, 35(3):1191–1200, 1998.
- [21] J. Windmolders and P. Dierckx. Subdivision of uniform Powell-Sabin splines. *Comput. Aided Geom. Design*, 16:301–315, 1999.
- [22] R. Zhang and G. Wang. Sharp bounds on the approximation of a Bézier polynomial by its quasi control polygon. *Comput. Aided Geom. Design*, 23(1):1–16, 2006.